Journal of The Electrochemical
Society

The Electrochemical Society
Advancing solid state & electrochemical science & technology

Electrochemical Preparation of Fine Powders of Nickel-Boron Alloys in Molten Chlorides for Magnetic Hydrogenation Catalysts

To cite this article: Junjun Peng *et al* 2015 *J. Electrochem. Soc.* **162** H271

Journal of The Electrochemical Society, **162** (4) H271-H277 (2015)

Electrochemical Preparation of Fine Powders of Nickel-Boron Alloys in Molten Chlorides for Magnetic Hydrogenation Catalysts

Junjun Peng,[a,b] Rui He,[a] Mingsheng Tan,[a] Yanpeng Dou,[b] Zhiyong Wang,[a] George Z. Chen,[a,c,*] and Xianbo Jin[a,z]

[a]*College of Chemistry and Molecular Sciences, Wuhan University, Wuhan, 430072, People's Republic of China*
[b]*College of Chemistry and Chemical Engineering, Wuhan Textile University, Wuhan, 430073, People's Republic of China*
[c]*Department of Chemical and Environmental Engineering, and Energy and Sustainability Research Division, Faculty of Engineering, University of Nottingham, Nottingham NG7 2RD, United Kingdom*

Fine powders of magnetic nickel-boron alloys were prepared for the first time by direct electrochemical reduction of the $2Ni_3(BO_3)_2/B_2O_3$, $Ni_3(BO_3)_2/NiO$ and $Ni_3(BO_3)_2/3NiO$ composite precursors in molten $CaCl_2$-NaCl at 700°C. Precursors with different nickel to boron atomic ratios ($R_{Ni/B} = 1$, 2 or 3) were synthesized by the sol-gel process followed by thermal annealing at 750°C. The reduction pathway, phase transformation and morphology of the samples electrolyzed at different voltages and times were analyzed by XRD, SEM, and EDX. When the applied voltage reached to 3.0 V, pure Ni_3B can be obtained from the oxide precursor with $R_{Ni/B} = 3$. However, the oxide precursors with $R_{Ni/B} = 1$ and 2 both resulted in mainly Ni_2B. It was found that all the precursors were firstly reduced to Ni metal and $Ca_3(BO_3)_2$, and then to Ni_3B, and finally to Ni_2B for $R_{Ni/B} = 1$ and 2. SEM observation showed that the prepared crystalline Ni_3B and Ni_2B powders consisted of uniform nodular particles with sizes of 200∼500 nm. These Ni-B alloys exhibited high catalytic activity to the hydrogenation reaction between p-nitrophenol and $NaBH_4$. Their good ferromagnetism allows them to be easily recovered and reused.

[DOI: 10.1149/2.0871504jes]

Manuscript submitted October 20, 2014; revised manuscript received January 30, 2015. Published February 6, 2015.

Metal borides with a boron covalent framework have interesting physical properties, such as high hardness, superconductivity, thermal stability, oxidation resistance, high melting points and outstanding permanent magnetism. They are widely used in various high-tech industries.[1] Metal borides also possess high catalytic activity to the hydrogenation reactions and hydrogen production.[2–4] Metal borides are prepared in three forms, namely, the bulk materials, the amorphous or crystalline powders. Each of them has its applied advantages. For example, nano-amorphous nickel borides have shown much higher activity and selectivity in the catalytic hydrogenation of organic substances such as benzene, p-chloronitrobenzene, and furfural.[5–7] The crystalline nickel borides can be used as diffusion barrier for Cu integrated circuit,[8] and also used as surface coating for the strengthening or corrosion prevention of the substrate.[9–10]

Although nickel borides can be easily prepared by the high temperature reaction between Ni and B,[11] it is quite difficult to convert the obtained bulk borides into fine powders. Nanometer Ni-B can be prepared by reaction between the borohydride and the nickel ions in a solution. For example, nano-amorphous Ni-B was synthesized in aqueous solutions,[12–13] and nano-crystalline Ni_3B was prepared at 300°C in tetraethylene glycol.[14] Alternatively, the solvothermal method in benzene resulted in nano-crystalline Ni-B as well.[15] However, these methods need expensive and toxic borohydrides serving both as the reducing agent and boron source.

Since late 1990s, it has been reported that metal, alloy and intermetallic powders can be directly prepared by electrolysis of solid precursors of metal compounds (e.g. oxides or sulfides) and mixed metal compounds respectively in high temperature molten salts.[16–24] This method is also capable of processing and production of nanomaterials for various applications such as enhancing catalytic and photoresponsive performances[17,25–28].

Metal borides could be also prepared by this process. However, the melting point of B_2O_3 (450°C) is much lower than the working temperatures (600°C ∼900°C) of the commonly used molten chloride salts such as $CaCl_2$ and LiCl. Therefore, B_2O_3 cannot be directly used as a precursor for electrolysis. It was reported that, by sintering the mixture of B_2O_3 and Fe_2O_3 at 900°C, Fe_3BO_6 could be obtained and used as solid source of B for the electrolysis. Subsequently, Fe-B alloy with a B content of about 4.6 wt% has been prepared at 850°C.[29]

In this paper, we report the preparation of fine crystalline powders of nickel borides by direct electrochemical reduction of the $2Ni_3(BO_3)_2/B_2O_3$, $Ni_3(BO_3)_2/NiO$ and $Ni_3(BO_3)_2/3NiO$ composites in molten $CaCl_2$-NaCl at 700°C. These precursors were synthesized by a sol-gel codeposition method and could be reduced quickly to Ni_3B and Ni_2B fine powders. We also report preliminary findings of the high catalytic activity of these ferromagnetic powders to the hydrogenation reaction of 4-nitrophenol (NO_2-C_6H_4-OH) in the aqueous solution of sodium borohydride ($NaBH_4$).

Materials and Methods

Preparation of oxide composite precursors.— All of the reagents were of the analytical grade and used as received. The composites with different nickel to boron atomic ratios ($R_{Ni/B} = 1, 2$ or 3) were prepared by the reaction between $Ni(NO_3)_2 \cdot 6H_2O$ and H_3BO_3 in aqueous solution with the presence of $C_6H_8O_7$ (citric acid) foaming agent.[30] After magnetic stirring for 2–3 h, the homogenous mixture was placed in an oven at 150°C for 12 h to obtain a dry gel, which was then calcinated at 750°C for 4 h in a muffle furnace. Finally, the samples were cooled to room temperature with oxide composite precursors generated. These oxide composites were denoted as $2Ni_3(BO_3)_2/B_2O_3$ ($R_{Ni/B} = 1$), $Ni_3(BO_3)_2/NiO$ ($R_{Ni/B} = 2$), $Ni_3(BO_3)_2/3NiO$ ($R_{Ni/B} = 3$) respectively.

Electrolysis of the composite precursors.— The oxide composite was pressed at 10 MPa into a cylindrical pellet (13 mm in diameter, 1.0–1.2 mm in thickness, ca. 0.5 g in mass), which was sintered at 300°C for 2 h. Then, the sintered pellet was wrapped with a foamed Ni layer and a Mo wire (0.18 mm in diameter) onto a Mo rod (2 mm in diameter, 1 m in length) that functioned as the current connector. This assembled electrode was used as the cathode and electrolyzed against a graphite rod anode at 700°C. The electrolyte was the $CaCl_2$-NaCl mixture at equi-molar ratio. Typically, anhydrous $CaCl_2$ (600 g, purity:>96 wt%, content of Mg and alkali metals: ∼0.3 wt%) and NaCl (291 g) were mixed and dried at 300°C before melting at 700°C in a graphite crucible placed in a stainless steel reactor under argon protection. Pre-electrolysis was performed at 2.6 V for 10 h between a nickel foil cathode and a graphite rod anode.

---

[*] Electrochemical Society Active Member.
[z] E-mail: xbjin@whu.edu.cn

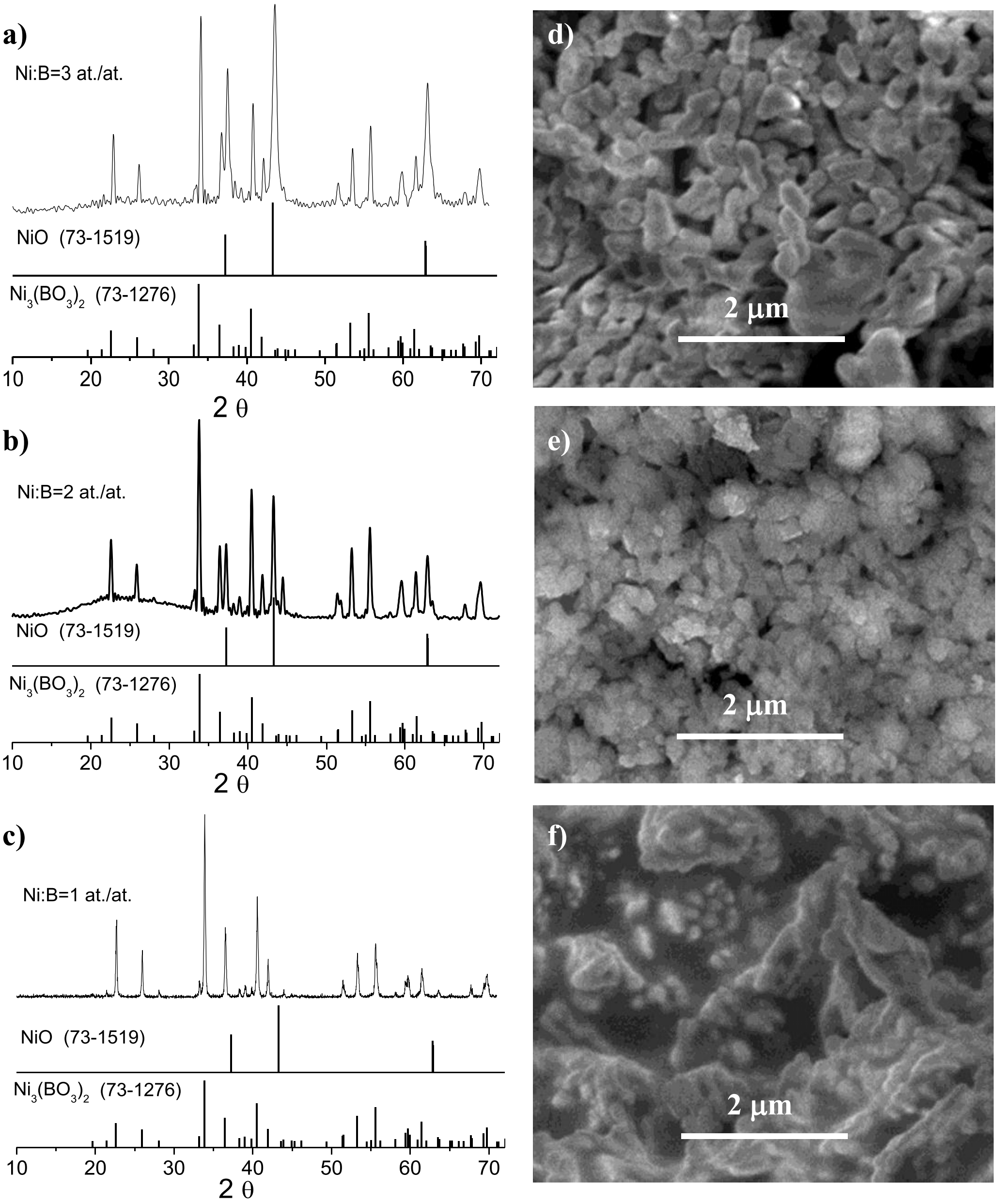

Figure 1. Powder XRD patterns and SEM images of different oxide precursors with different atomic ratios of Ni/B: a, d) $Ni_3(BO_3)_2/3NiO$, b, e) $Ni_3(BO_3)_2/NiO$ and c, f) $2Ni_3(BO_3)_2/B_2O_3$.

Catalytic hydrogenation of 4-NP.— Investigations of the catalytic activity of the prepared nickel boride powders were pursued using the reduction of 4-nitrophenol (4-NP) to 4-aminophenol (4-AP) by $NaBH_4$ as a model reaction at 26°C. Aqueous 4-NP solution (50 mL, 0.266 mM) was mixed with fresh $NaBH_4$ (13.3 mM). The prepared nickel borides powder (20 mg) was dispersed in the mixture. UV-Vis absorption spectra (TU-1901, Beijing Purkinje General Instrument Co., Ltd.) were recorded to determine the variation of the maximum absorption intensity in the wavelength range of 250–500 nm.

Equipments and characterization.— Precursors and products were characterized by X-ray diffraction spectroscopy (XRD, Shimadzu X-ray 6000 with Cu $K\alpha_1$ radiation at $\lambda = 1.5405$ Å), scanning electron microscopy (SEMFEI Sirion Field Emission Gun SEM), and energy dispersive X-ray spectroscopy (EDAX, GENESIS 7000). A camera was used to record the color change of 4-NP during the catalytic reduction experiment.

Results and Discussion

The oxide composite precursors.— Because of the low melting point of B_2O_3 (450°C), if metal borides, such as Ni-B, are targeted by the electrolysis of solid compound precursor in molten chlorides, it is desirable to react the B_2O_3 with NiO to form the compounded oxides with higher melting points, such as $Ni_3(BO_3)_2$.[32] Although the $Ni_3(BO_3)_2$ can be easily prepared by annealing NiO in molten B_2O_3 at about 1200°C, the generated large grains of the compound may be unfavorable for the subsequent electrolytic reduction. Alternatively, here, the sol-gel method was applied to prepare the nickel borate with fine particle sizes.[30] In this study, since in the $Ni_3(BO_3)_2$ there is $R_{Ni/B} = 1.5$, to get a ratio of 1, 2 or 3, excess source of B or Ni should be added during the sol-gel deposition process, thus composites of $2Ni_3(BO_3)_2/B_2O_3$, $Ni_3(BO_3)_2/NiO$, $Ni_3(BO_3)_2/3NiO$ would be collected after the calcination.

Fig. 1a to 1c show the XRD patterns of the prepared oxide composites. When $R_{Ni/B} = 2$ or 3, $Ni_3(BO_3)_2$ and NiO were the dominant

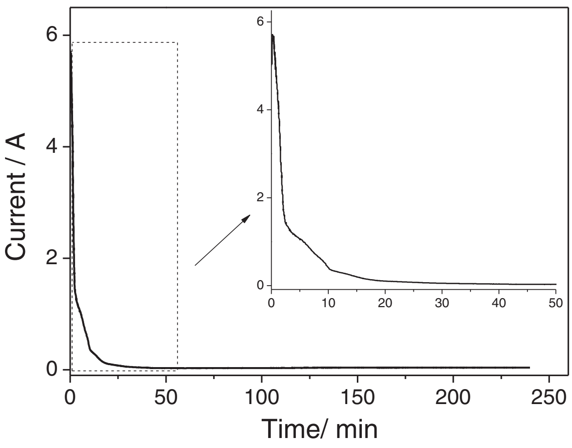

Figure 2. Typical current-time plot of electrolysis of the $Ni_3(BO_3)_2/3NiO$ pellet (0.5 g in mass) under a cell voltage of 3.0 V against a graphite rode anode in 700°C $CaCl_2$-NaCl melts.

phases in the composite. Fig. 1d and 1e indicate that the generated $Ni_3(BO_3)_2/3NiO$ and $Ni_3(BO_3)_2/NiO$ composites were in a uniform morphology, with a porous structure building from fine particles of 0.1–1 μm in size.

For $R_{Ni/B} = 1$, boron oxide should be present in the $2Ni_3(BO_3)_2/B_2O_3$ composite. Since boron oxide is in amorphous structure in nature, it cannot be detected by XRD, and Fig. 1c shows only the pattern of $Ni_3(BO_3)_2$. The SEM image in Fig. 1f shows a lot of particles fused by dense substance, which may be amorphous B_2O_3.

Electrolysis of $Ni_3(BO_3)_2/3NiO$ in molten $CaCl_2$-NaCl at 700°C.— The $Ni_3(BO_3)_2/3NiO$ cathodes were electrochemically reduced by applying a cell voltage of 3.0 V for different electrolysis times. Fig. 2 shows the typical current-time plots at 700°C in $CaCl_2$-NaCl. The trend of current was very similar to those of other metal oxides in some reported work.[21,24,31,33] The inset of Fig. 2 shows that the current rose to a high value (ca. 5.66 A for one pellet with a diameter of 1.3 cm) in the first 1 min of electrolysis, and then decreased quickly through a few plateau in the next 40 minutes, indicating a fast reduction process, and at last declined gradually until it reached a background current of about 40 mA. The larger reduction current of the $Ni_3(BO_3)_2/3NiO$ composite in comparison with other oxides[21,24,31,33] could be attributed to (1) the thermodynamic advantage for the reduction of NiO ($2NiO = 2Ni + O_2$, $\Delta G = 301.8$ kJ/mol vs., for example, $TiO_2 = Ti + O_2$, $\Delta G = 767.4$ kJ/mol at 700°C) and (2) the electronic conductivity of NiO, which allows the happening of electrochemical reaction at the solid | electrolyte interface. However, the metal | oxide | electrolyte three-phase interlines (3PIs) may be still most favorable to the reduction considering the higher conductivity of the metal. The reduction of the interior oxide of the pellet could have resulted in the following current decrease due to the increasing mass transfer difficulty.

There are about three current stages as reflected by the slope changes of the current-time curve shown in Fig. 2, indicating the reduction going through a number of mechanistic and/or kinetic steps. XRD analysis was performed to identify the respective intermediate products obtained after different electrolysis times at 3.0 V. As shown in Fig. 3, the XRD pattern of the 5-minute electrolysis product shows distinctive peaks of nickel, accompanied by small peaks of $Ca_3(BO_3)_2$. Both the XRD peaks of NiO and $Ni_3(BO_3)_2$ decreased significantly compared to the pattern of the precursor shown in Fig. 1a, suggesting the rapid reduction of NiO and $Ni_3(BO_3)_2$ to nickel. The reduction of borate ions should be slower, which converted into $Ca_3(BO_3)_2$.[29] Weak peaks of $Ca(OH)_2$ can also be found. It was suggested that a quick release of O^{2-} from the metal oxide could result in the precipitation of CaO,[34–36] which would hydrolyze to $Ca(OH)_2$ during water washing.

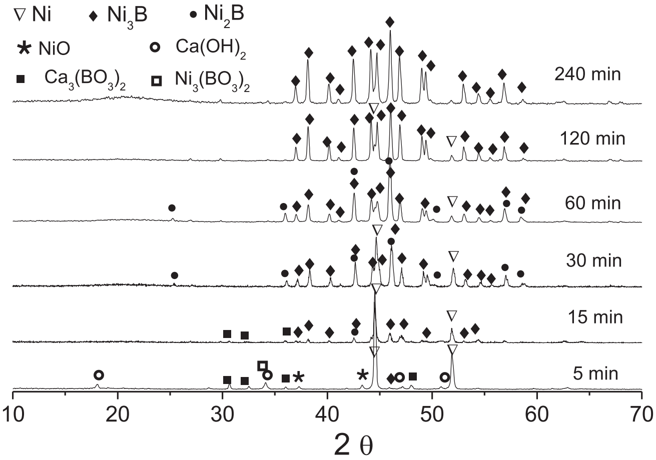

Figure 3. Powder X-ray diffraction patterns of products from electrolysis of the $Ni_3(BO_3)_2/3NiO$ at 3.0 V for different time as indicated in 700°C $CaCl_2$-NaCl melts.

The 5-minute electrolysis sample was further studied by the SEM and EDX analysis, and the results are shown in Fig. 4. It can be seen some large particles with sizes of 2–5 μm blending with some small particles with sizes less than 1 μm, which contain Ca, Ni, B, Pt, and O as determined by the inserted EDX spectrum. The Pt element came from the sputter treatment of the sample for SEM observation. According to the point element analysis with EDX, the large particle might be $Ca_3(BO_3)_2$, and the small particle might be Ni or Ni_3B.

After 15 minutes electrolysis, the XRD peaks of NiO and $Ni_3(BO_3)_2$ disappeared, indicating the complete metallization of the nickel ions. At the same time, both the peaks of Ni and $Ca_3(BO_3)_2$ weakened, suggesting the reduction of $Ca_3(BO_3)_2$ on Ni and the formation of nickel borides. After 30 minutes, the product only showed the XRD peaks of Ni, Ni_2B and Ni_3B, indicating the almost completion of the electrochemical reduction. This is in line with the I-t curve as shown in Fig. 2, where the current declined to a background value after the 30-minute electrolysis. The left electrolysis would reduce the trace of oxides but might mainly contribute to the homogenization of the product by the reaction between Ni and Ni_2B. It can be seen that the Ni and Ni_2B phases gradually decreased, and Ni_3B become dominant in the product after 120-minute electrolysis. The 4-h electrolysis resulted in a yield of Ni_3B higher than 95%.

Based on the above discussion, the electro-reduction of $Ni_3(BO_3)_2/3NiO$ to Ni_3B in molten $CaCl_2$-NaCl should have pro-

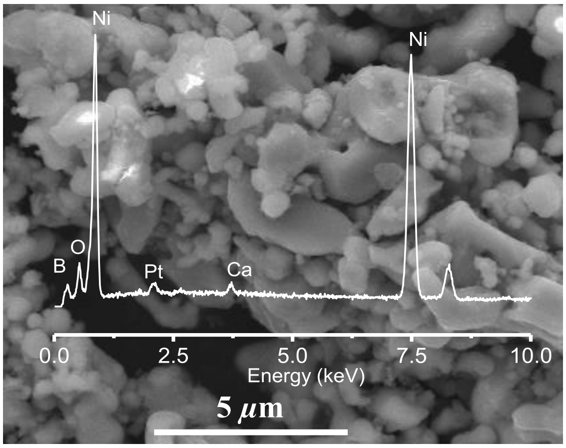

Figure 4. The SEM image and corresponding EDX spectra of the electrolysis product from the $Ni_3(BO_3)_2/3NiO$ at 3.0 V for 5 min.

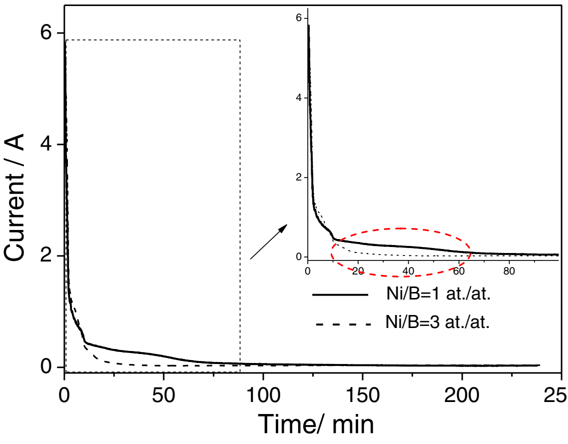

Figure 5. Typical current-time plots of electrolysis of $2Ni_3(BO_3)_2/B_2O_3$ at 3.0 V and 700°C in molten $CaCl_2$-NaCl. The dash line shows that recorded from the electrolysis of $Ni_3(BO_3)_2/3NiO$ as shown in Fig. 1 for comparison.

ceeded through the following steps,

$$NiO + 2e = Ni + O^{2-} \quad [1]$$

$$Ni_3(BO_3)_3 + 3Ca^{2+} + 6e = 3Ni + Ca_3(BO_3)_3 \quad [2]$$

$$Ca_3(BO_3)_2 + 6Ni + 6e = 2Ni_3B + 3Ca^{2+} + 6O^{2-} \quad [3]$$

$$Ca_3(BO_3)_2 + 4Ni + 6e = 2Ni_2B + 3Ca^{2+} + 6O^{2-} \quad [4]$$

$$Ni_2B + Ni = Ni_3B \quad [5]$$

Reaction 4 might occur in cases there were local uneven distribution between Ni and $Ca_3(BO_3)_2$. The generated Ni_2B would convert to Ni_3B through a solid state reaction with Ni (Reaction 5). This solid reaction took about 90 minutes as reflected in Fig. 3, and finally Ni_3B was produced from the $Ni_3(BO_3)_2/3NiO$ precursor.

Electrolysis of the $2Ni_3(BO_3)_2/B_2O_3$ and $Ni_3(BO_3)_2/NiO$.— Fig. 5 shows typical current-time plots for the electrolysis of $2Ni_3(BO_3)_2/B_2O_3$ in the $CaCl_2$-NaCl melt at 3.0 V and 700°C. The plots recorded from the electrolysis of $Ni_3(BO_3)_2/3NiO$ were also displayed for comparison. Compared to $Ni_3(BO_3)_2/3NiO$, there was a long and low current plateau (from 15 min to 50 min) emerging during the electrolysis of $2Ni_3(BO_3)_2/B_2O_3$. This plateau current can be attributed to slow reduction of $Ca_3(BO_3)_2$, considering the large amount of borate ions in the $2Ni_3(BO_3)_2/B_2O_3$ composite.

Fig. 6a shows the phase transformation during the electrolysis of $2Ni_3(BO_3)_2/B_2O_3$. It can be seen that similar to the electrolysis of $Ni_3(BO_3)_2/3NiO$, both Ni and $Ca_3(BO_3)_2$ formed in the first 5 min electrolysis, suggesting again the relatively fast reduction of $Ni_3(BO_3)_2$ to Ni and borate ions. However, the 15-min electrolysis product still showed the distinct XRD pattern of $Ni_3(BO_3)_2$, probably indicating that the reduction of $Ni_3(BO_3)_2$ was slightly slower than the reduction of NiO if compared to Fig. 3. At the same time, the amount of $Ca_3(BO_3)_2$ increased due to the reaction between the calcium ions in the melt and the released borate ions from the $Ni_3(BO_3)_2$. Another argument might be that there was more Ni generated initially from the $Ni_3(BO_3)_2/3NiO$ composite, which would be favorable for the reduction of both $Ni_3(BO_3)_2$ and $Ca_3(BO_3)_2$.

The slower reduction kinetics of $Ca_3(BO_3)_2$ was further confirmed by the experimental results from electrolysis at different cell voltages. As shown in Fig. 6b, after electrolysis at 2.0 V for 2 hours, the XRD peaks of $Ni_3(BO_3)_2$ completely disappeared, and the XRD pattern

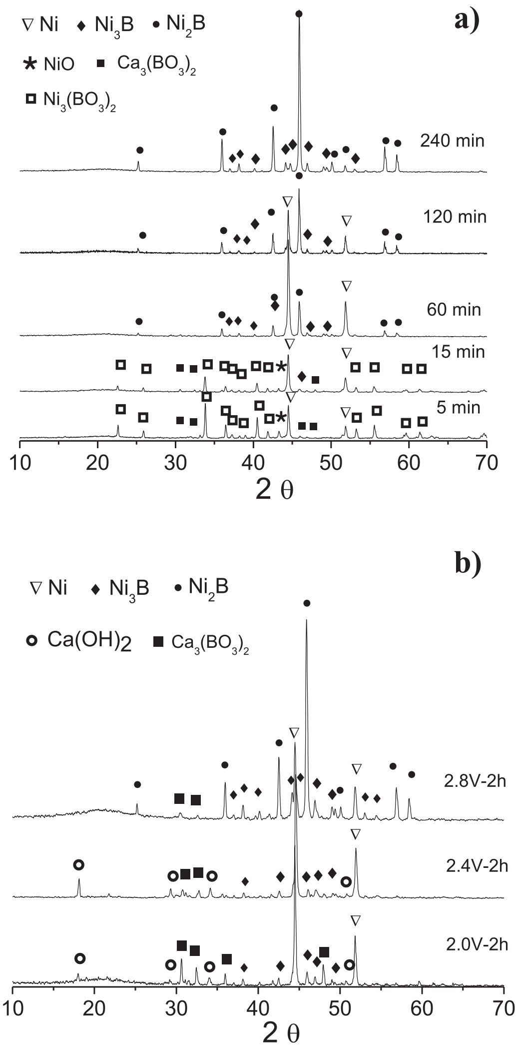

Figure 6. Powder X-ray diffraction patterns of products from electrolysis of the $2Ni_3(BO_3)_2/B_2O_3$ at 3.0 V for different time (a) or at different voltages for 2 h (b) as indicated in700°C $CaCl_2$-NaCl melts.

shows mainly metallic Ni and $Ca_3(BO_3)_2$. It seems that increasing the cell voltage to 2.4 V had little help to the reduction of $Ca_3(BO_3)_2$, considering that Ni was still the predominant product and only a small amount of Ni-B alloys formed. The effective reduction of $Ca_3(BO_3)_2$ could occur at 2.8 V, and the Ni-B alloys became predominant after the 2 h electrolysis as evidenced by the XRD analysis (Fig. 6b). At the same time, the XRD peaks of Ni weakened significantly. However, there were still small XRD peaks of $Ca_3(BO_3)_2$ in the 2 h electrolysis product, indicating again the great difficulty in the reduction of $Ca_3(BO_3)_2$ even at a cell voltage of 2.8 V.

The reduction of $Ca_3(BO_3)_2$ could be accelerated by imposing a higher cell voltage. As can be seen in Fig. 6a, the electrolysis after 60 minutes at 3.0 V product shows no XRD peaks of $Ca_3(BO_3)_2$, indicating most of the oxides in the cathode have been reduced. Similar to the electrolysis of $Ni_3(BO_3)_2/3NiO$, the post-electrolysis has mainly contributed to the alloying process, with the metallic Ni converting to Ni_2B gradually. After the 4 h electrolysis, the XRD peaks of Ni_2B became dominant in Fig. 6a, while those of Ni almost disappeared.

It should be pointed out that although the atomic ratio of Ni/B in the $2Ni_3(BO_3)_2/B_2O_3$ was designed to be 1:1, as discussed above, the final electrolysis product was mainly Ni_2B. No NiB product was detected by the XRD analysis. The formation of NiB could have suffered from the thermodynamic difficulty in comparison to those of Ni_3B and Ni_2B considering electrode reactions (6–12), where the thermodynamic potentials were referred to the equilibrium potential of Ca/Ca^{2+}. Reaction 14 indicates that the reduction of NiO to Ni can be easily realized considering a thermodynamic potential of as positive as 1.98 V. In comparison, the reduction of $Ca_3(BO_3)_2$ to B with $E^0 = 0.547$ V would be much more difficult. However, it would be favorable for the reduction of $Ca_3(BO_3)_2$ on Ni with Ni-B alloys formed. Particularly, the formation potential of Ni_3B positively shifts to about 0.816 V, and the fast electrolysis of $Ni_3(BO_3)_2$/3NiO to Ni_3B has been observed as discussed above. The reduction potential (0.677 V) of $Ca_3(BO_3)_2$ on Ni to NiB is also higher, but Ni_3B or Ni_2B would form preferentially. Then, the potentials for the consequent reduction of $Ca_3(BO_3)_2$ on Ni_3B and Ni_2B negatively shift to 0.608 and 0.595 V respectively, suggesting increasing difficulty in the generation of NiB.

$$\mathrm{Ca} + 2\mathrm{e} = \mathrm{Ca}^{2+} \quad E^0 = 0\,\mathrm{V} \tag{6}$$

$$\mathrm{Ca_3(BO_3)_2} + 6\mathrm{e} = 3\mathrm{CaO} + 2\mathrm{B} + 3\mathrm{O}^{2-} \quad E^0 = 0.547\,\mathrm{V} \tag{7}$$

$$\mathrm{Ca_3(BO_3)_2} + 2\mathrm{Ni_2B} + 6\mathrm{e} = 3\mathrm{CaO} + 4\mathrm{NiB} + 3\mathrm{O}^{2-} \quad E^0 = 0.595\,\mathrm{V} \tag{8}$$

$$\mathrm{Ca_3(BO_3)_2} + \mathrm{Ni_3B} + 6\mathrm{e} = 3\mathrm{CaO} + 3\mathrm{NiB} + 3\mathrm{O}^{2-} \quad E^0 = 0.608\,\mathrm{V} \tag{9}$$

$$\mathrm{Ca_3(BO_3)_2} + 4\mathrm{Ni_3B} + 6\mathrm{e} = 3\mathrm{CaO} + 6\mathrm{Ni_2B} + 3\mathrm{O}^{2-} \quad E^0 = 0.645\,\mathrm{V} \tag{10}$$

$$\mathrm{Ca_3(BO_3)_2} + 2\mathrm{Ni} + 6\mathrm{e} = 3\mathrm{CaO} + 2\mathrm{NiB} + 3\mathrm{O}^{2-} \quad E^0 = 0.677\,\mathrm{V} \tag{11}$$

$$\mathrm{Ca_3(BO_3)_2} + 4\mathrm{Ni} + 6\mathrm{e} = 3\mathrm{CaO} + 2\mathrm{Ni_2B} + 3\mathrm{O}^{2-} \quad E^0 = 0.759\,\mathrm{V} \tag{12}$$

$$\mathrm{Ca_3(BO_3)_2} + 6\mathrm{Ni} + 6\mathrm{e} = 3\mathrm{CaO} + 2\mathrm{Ni_3B} + 3\mathrm{O}^{2-} \quad E^0 = 0.816\,\mathrm{V} \tag{13}$$

$$\mathrm{NiO} + 6\mathrm{e} = \mathrm{Ni} + \mathrm{O}^{2-} \quad E^0 = 1.98\,\mathrm{V} \tag{14}$$

The mismatch in the atomic ratio of Ni/B between the precursor and the outcomes for the electrolysis of $2Ni_3(BO_3)_2/B_2O_3$ could be due to the dissolution of B_2O_3 into the melt at 700°C, whose melting point is only 450°C. The product was a mixture of Ni_2B and Ni_3B with a nickel to boron atomic ratio higher than 2, suggesting some of the $Ca_3(BO_3)_2$ or borate ions could have also slightly dissolved. Similar phenomenon was observed during the electrolysis of $Ni_3(BO_3)_2$/NiO aiming to Ni_2B powders. After 4 h electrolysis at 3.0 V, although the product consisted of mainly Ni_2B, there exist clear XRD peaks of Ni_3B in Fig. 7a, whose content was higher than in the electrolysis product from $2Ni_3(BO_3)_2/B_2O_3$ as expected.

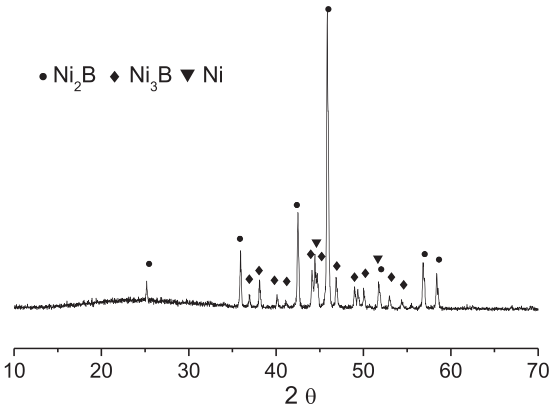

Figure 7. Powder X-ray diffraction pattern of the product from 4 h electrolysis of the $Ni_3(BO_3)_2$/NiO at 3.0 V and 700°C in $CaCl_2$-NaCl melt.

On the other hand, the yields from the electrolysis of $Ni_3(BO_3)_2$/NiO and $2Ni_3(BO_3)_2/B_2O_3$ were about 86% and 82% respectively, probably due to the loss of B according to the XRD analysis. These observations suggested that more source of B in the oxide composite precursor would be needed for the preparation of pure Ni_2B powders through this electrolysis method.

Catalytic performance of the crystalline Ni-B alloy powders.— The above relatively purer Ni_3B and Ni_2B electrolyzed from the $Ni_3(BO_3)_2$/3NiO and $2Ni_3(BO_3)_2/B_2O_3$ were tested to be used as catalysts for the reduction hydrogenation of p-nitrophenol (4-NP). As shown in Figure 8, both the Ni_3B and Ni_2B exhibited uniform nodular particles with sizes of 200∼500 nm, which might be able to provide large surface area for the heterogeneous catalysis. Small amounts of O in the two borides can also be detected by the EDX analysis. This was usually ascribed to the formation of thin layer coating of oxides on the Ni_3B particles formed during water washing.[25–28,37,38]

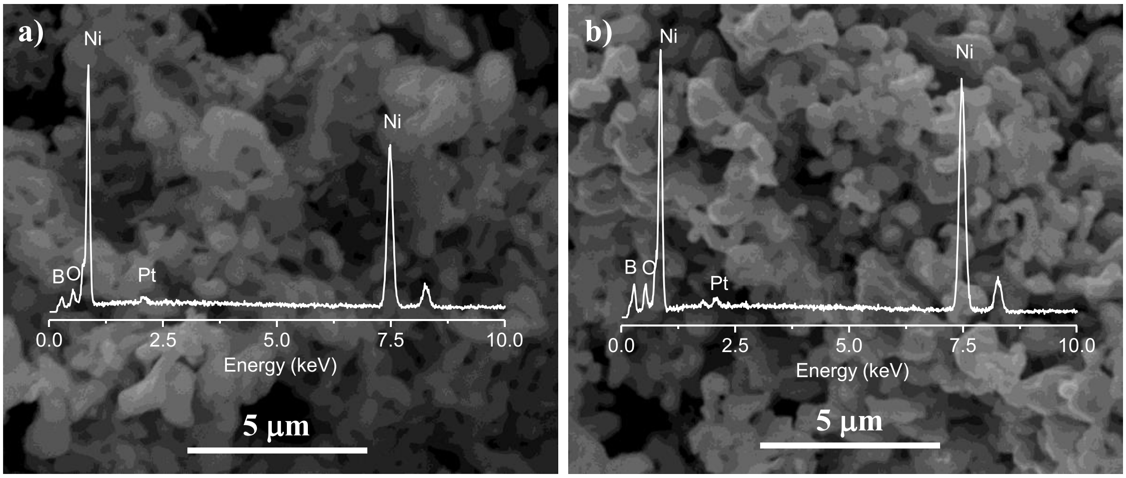

Figure 8. SEM images of (a) the Ni_3B from the 2 h electrolysis of $Ni_3(BO_3)_2$/3NiO and (b) Ni_2B from the 4 h electrolysis of $2Ni_3(BO_3)_2/B_2O_3$ at 3.0 V and 700°C in $CaCl_2$-NaCl melt.

4-Aminophenol (4-AP) has many important applications, which can be used as analgesic and antipyretic drugs, photographic developer, corrosion inhibitor, anticorrosion lubricant, and so on.[39] 4-AP was usually prepared by reduction of 4-NP with $NaBH_4$ in the presence of catalysts.[40,41] The catalytic reduction process can be represented as,

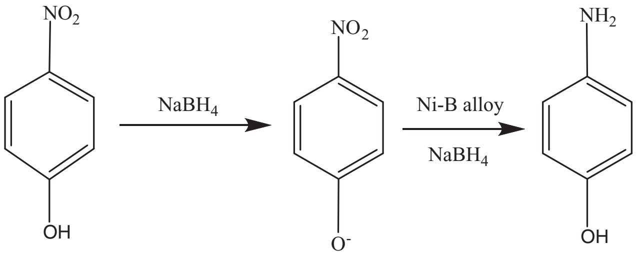

It is interesting that the synthesized Ni_3B and Ni_2B powders are ferromagnetic as shown in Fig. 9a. This will be very beneficial for the reclamation of these catalysts. In this study, during the catalytic reaction between the 4-NP and NaBH under magnetic stirring, the Ni-B alloy powders were always caught on the stirring bar. Since there will be a remarkable color change from the 4-NP solution (light yellow) to 4-AP (colorless), UV-vis analysis was used to monitor the reduction process (Fig. 9b). Aqueous solution of 4-NP shows a distinct spectra profile with an absorption maximum at 317 nm, which shifts to 400 nm in the presence of $NaBH_4$ due to the formation of the 4-nitrophenolate ion.[42] Without addition of the Ni-B alloy catalysts, the color of aqueous solution kept almost unchanged during standing at room temperature. The color changed immediately after the addition of the Ni-B alloys. It can be seen from Fig. 9b that the time-dependent absorption spectra show a decrease in the intensity of the absorption peak at 400 nm and a concomitant increase of a new peak at 298 nm, which is the sign of the generation of 4-AP. After about 30 minutes, the peak due to the nitro compound was no longer observed, indicating the completion of the reduction of the 4-NP.

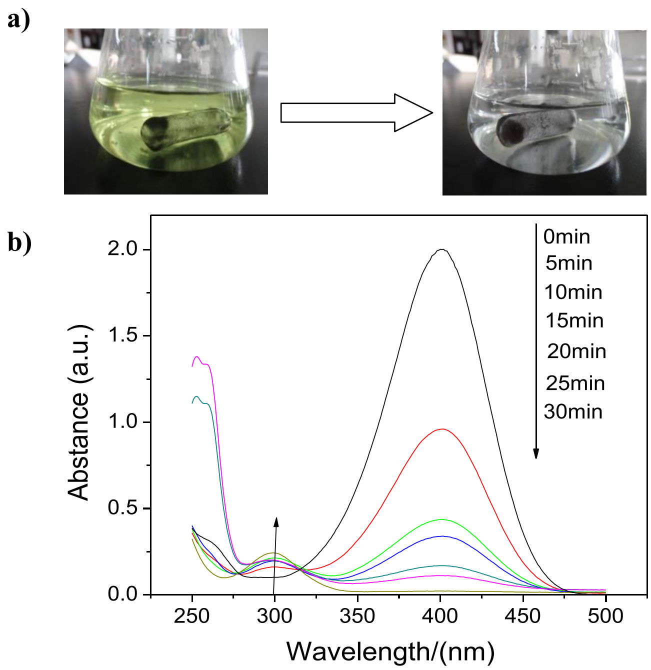

Figure 9. a) The photos of light yellow 4-NP aqueous solution and the colorless 4-AP solution after hydrogenation reaction with Ni-B alloy catalysts. b) Typical UV-vis spectra shows the gradual reduction of 4-NP by $NaBH_4$ in aqueous solution at 26°C with the electrolytic Ni_3B powder serving as the catalyst.

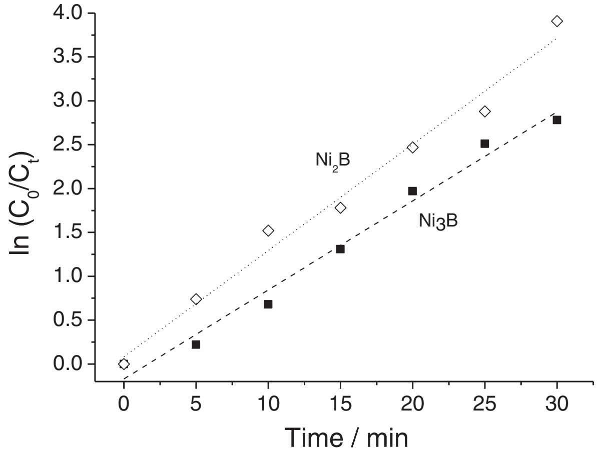

Figure 10. Plots of $\ln(C_0/C_t)$ versus the reaction time for the catalytic hydrogenation reduction of 4-NP in the presence of the electrolysis obtained crystalline Ni_3B and Ni_2B powders.

The reaction rate was assumed to be independent of the concentration of sodium borohydride since this reagent was used in large excess. Therefore, the kinetic data could be fit with the first-order rate law:[43]

$$\ln(C_0/C_t) = kt \qquad [15]$$

Since the absorbance of 4-NP is proportional to its concentration, the ratio A_0/A_t (A_0 the initial absorbance and A_t the absorbance at time t of the solution at 400 nm) should be equal to the ratio of the corresponding concentrations of 4-NP (C_0/C_t). Indeed, a good linear relationship between $\ln(C_0/C_t)$ and reaction time was found for the catalytic reduction of 4-NP (Fig. 10). The regression analysis suggest rate constants k of about 0.12 and 0.10 min^{-1} in the presence of Ni_2B and Ni_3B powders respectively, which are comparable to the catalytic activity of nickel nanoparticles.[44]

This ferromagnetic property of the nano-crystalline Ni_3B and Ni_2B makes them distinguished from those amorphous Ni-B alloy catalysts, which were non-magnetic and difficult to be recaptured from the reaction system. The crystalline Ni-B alloys particularly Ni_3B display good magnetic property.[45] Pure Ni_2B is non-ferromagnetic in nature. Here the electrolysis prepared Ni_2B powders showed enough ferromagnetism to be captured by the stirring bar, probably due to they were actually a mixture of Ni_2B and Ni_3B. In addition, the crystalline Ni_3B and Ni_2B alloy catalysts would be more stable than those amorphous Ni-B alloys. During repeated use as hydrogenation catalysts, spontaneous crystallization of the amorphous alloys was often found and could lead to segregation of Ni and B.[46] These suggest that the electrolysis generated nano-crystalline Ni-B alloys are promising hydrogenation catalysts. In future studies, the stability and cyclicity of these nano-crystalline Ni-B alloy catalysts need to be tested, and the correlation between the magnetic nature and the catalytic performance could be an interesting topic for the magnetic catalysts.

Conclusions

In summary, we have prepared crystalline Ni_3B and Ni_2B fine powders by direct electrochemical reduction of $2Ni_3(BO_3)_2/B_2O_3$, $Ni_3(BO_3)_2/NiO$ and $Ni_3(BO_3)_2/3NiO$ composites precursors in molten $CaCl_2$-NaCl at 700°C. It was found that both the NiO and $Ni_3(BO_3)_2$ could be easily reduced to Ni, whereas, the reduction of borate ions were more difficult, which precipitated as $Ca_3(BO_3)_2$ in the solid cathode. The reduction of borate ions or $Ca_3(BO_3)_2$ on Ni formed the Ni_3B and Ni_2B alloys finally. Ni_3B alloy was generated by the fast reduction of $Ni_3(BO_3)_2/3NiO$. During the electrolysis of $2Ni_3(BO_3)_2/B_2O_3$, B_2O_3 was likely to have dissolved into the $CaCl_2$-NaCl melt due to its low melting point. However, slightly dissolution of $Ca_3(BO_3)_2$

into the melt might have occurred, considering both the electrolysis products from the $2Ni_3(BO_3)_2/B_2O_3$ and $Ni_3(BO_3)_2/NiO$ contained some Ni_3B. Relatively pure Ni_2B was obtained by electrolysis of $2Ni_3(BO_3)_2/B_2O_3$ at a cell voltage of 3.0 V. Both the prepared crystalline Ni_3B and Ni_2B powders consisted of uniform nodular particles with sizes of 200∼500 nm. These crystalline alloys showed good ferromagnetism and high catalytic activity to hydrogenation reduction of p-nitrophenol by $NaBH_4$. These findings promise an effective approach for preparation of crystalline Ni-B nanometer powders as hydrogenation catalysts.

Acknowledgments

This work is supported by NSFCs (21173161, 20973130), the China Postdoctoral Science Foundation (20110491184), the MOE Program (NCET-11-0397), Science and Technology Research Programs for Excellent Young Talents of Educational Commission of Hubei Province (Q20111604), and the Fundamental Research Funds for the Central Universities of Wuhan University.

References

1. X. J. Zhen, *Metal borides and boron alloys*, Chemistry Industry Press, Beijing, 9–14 (2012).
2. Y. Zhu, F. Liu, W. Ding, X. Guo, and Y. Chen, , *Angew. Chem.*, **118**, 7369 (2006).
3. N. Pate, R. Fernandes, G. Guella, and A. A Miotello, *Appl. Catal. B: Environ.*, **140–141**, 125 (2013).
4. S Carenco, D Portehault, and C Boissière et al., *Chem. Rev.*, **113**, 7981 (2013).
5. Z. B. Yu, M. H. Qiao, H. X. Li, and J. F. Deng, *Appl. Catal. A: Gen.*, **163**, 1 (1997).
6. L. F. Chen and Y. W. Chen, *Ind. Eng. Chem. Res.*, **45**, 8866 (2006).
7. H. X. Li, X. F. Chen, M. H. Wang, and Y. P. Xu, *Appl. Catal. A: Gen.*, **225**, 13 (2002).
8. J. W. Choi, G. H. Hwang, W. K. Han, and S. G. Kang, *Appl. Surf. Sci.*, **253**, 2171 (2006).
9. K. S. Weil, J. Y. Kim, G. Xia, J. Coleman, and Z. G. Yang, *Surf. Coat. Technol.*, **201**, 4436 (2006).
10. S. Ziyuan, W. Deqing, and D. Zhimin, *Appl. Surf. Sci.*, **253**, 1051 (2006).
11. N. N. Greenwood, R. V. Parish, P. Thornton, and Metal borides, *Q. Rev. Chem. Soc.*, **20**, 441 (1966).
12. Y. C. Liu, C. Y. Huang, and Y. W. Chen, *J. Nanoparticle Res.*, **8**, 223 (2006).
13. J Yu, L Wang, Y Wang, H Dong, and H Yang, *J. Electrochem. Soc.*, **151**, A1124 (2004).
14. Z. L. Schaefer, X. Ke, and P. Schiffer., *J. Phys. Chem. C.*, **112**, 19846 (2008).
15. X. Feng, Y. J. Bai, B. Lü, Y. R. Zhao, and J. Yang , *Inorg. Chem. Commun.*, **7**, 189 (2004).
16. G. Z. Chen, D. J. Fray, and T. W. Farthing, *Nature*, **407**, 361 (2000).
17. T. Wang, G. H. Gao, X. B. Jin, H. Chen, J. J. Peng, and G. Z. Chen, *Electrochem. Commun.*, **13**, 1492 (2011).
18. R. Bhagat, D. Dye, S. L. Raghunathan, R. J. Talling, D. Inman, B. K. Jackson, K. K. Rao, and R. J. Dashwood, *Acta Mater.*, **58**, 5057 (2010).
19. D. Sri Maha Vishnu, N. Sanil, L. Shakila, G. Panneerselvam, R. Sudha, K. S. Mohandas, and K. Nagarajan, *Electrochim. Acta*, **100**, 51 (2013).
20. R Bhagat, M Jackson, and D Inman. , *J. Electrochem. Soc.*, **156**, E1 (2009).
21. C. Schwandta, D. T. L. Alexander, and D. J. Fray, *Electrochim. Acta*, **54**, 3819, (2009).
22. S. M. Jeong, H. Y. Yoo, J. M. Hur, and C. S. Seo, *J. Alloys. Compd.*, **452**, 27 (2008).
23. D. J. S. Hyslop, A. M. Abdelkader, A. Cox, and D. J. Fray, *Acta. Mater.*, **58**, 3124 (2010).
24. D. T. L. Alexander, C. Schwandt, and D. J. Fray, *Electrochim. Acta*, **56**, 3286 (2011).
25. H. Y. Yin, W. Xiao, X. H. Mao, W. F. Wei, H. Zhu, and D. H. Wang, *Electrochimi. Acta.*, **102**, 369 (2013).
26. J. Y. Yang, S. G. Lu, S. R. Kan, and X. J. Zhang, *J. Du. Chem. Commun.*, **22**, 3273 (2009).
27. W. Xiao, X. B. Jin, and G. Z. Chen, *J. Mater. Chem. A.*, **1**, 10243 (2013).
28. Y. Nishimura, T. Nohira, K. Kobayashi, and R. Hagiwara, *J. Electrochem. Soc.*, **158**, E55 (2011).
29. T. Örs, S Tan, T. Öztürk, and I. Karakaya, *J. Mater. Sci.*, **44**, 3514 (2009).
30. A. M. Chen, F. C. Hu, P. Gu, and Z. M. Ni, *Chinese. J. Inorg. Chem.*, **27**, 30 (2011).
31. J. J. Peng, K. Jiang, W. Xiao, D. H. Wang, and X. B. Jin, *Chem. Mater.*, **20**, 7274 (2008).
32. J. Pardo, M. Martinez-Ripoll, and S. García-Blanco, *Acta Cryst. B.*, **30**, 37 (1974).
33. D. J. S. Hyslop, A. M. Abdelkader, A. Cox, and D. J. Fray, *Acta. Mater.*, **58**, 3124 (2010).
34. R. Bhagat, D. Dye, S. L. Raghunathan, R. J. Talling, D. Inman, B. K. Jackson, K. K. Rao, and R. J. Dashwood, *Acta. Mater.*, **58** 5057 (2010).
35. H. P. Gao, X. B. Jin, S. W. Zou, F. Z. Ling, J. J. Peng, Z. Y. Wang, and G. Z. Chen, *Electrochim. Acta*, **107**, 261 (2013).
36. H. L. Chen, Y. Zeng, W. Li, J. J. Peng, X. B. Jin, and G. Z. Chen, *Electrochem. Comm.*, **26**, 33 (2013).
37. T. Wu, X. B. Jin, W. Xiao, X. H. Hu, and G. Z. Chen, *Chem. Mater.* **19**,153 (2007).
38. T. Wu, W. Xiao, X. B. Jin, C. Liu, D. H. Wang, and G. Z. Chen, *Phy. Chem. Chem. Phy.*, **10**, 1809 (2008).
39. Y. Du, H. Chen, R. Chen, and N. Xu, *Appl. Catal. A.*, **277**, 259 (2004).
40. J. R. Chiou, B. H. Lai, K. C. Hsu, and D. H. Chen, *J. Hazard. Mater.*, **248–249**, 394 (2013).
41. J. Li, C. Liu, and Y. J. Liu, *J. Mater. Chem.*, **22**, 8426 (2012).
42. S. Wunder, F. Polzer, Y. Lu, Y. Mei, and M. Ballauff, *J. Phys. Chem. C.*, **114**, 8814 (2010).
43. W. Zhang, F. Tan, W. Wang, X. L. Qiu, Q. X. Liang, and J. G. Chen, *J. Hazard. Mater.*, **217–218**, 36 (2012).
44. N. Sahiner, H. Ozay, O. Ozay, and N. Aktas, *Applied Catalysis A: General*, **385**, 201 (2010).
45. I. Baskaran, R. S. Kumar, T. S. N. S. Narayanan, and A. Stephen, *Surface & Coatings Technology*, **200**, 6888 (2006).
46. H. X. Li, H. Li, W. L. Dai, and M. H. Qiao, *Applied Catalysis A: General*, **238**, 119 (2003).